Carbohydrate Polymers 82 (2010) 337–345

Contents lists available at ScienceDirect

Carbohydrate Polymers

journal homepage: www.elsevier.com/locate/carbpol

Green nanocomposites based on thermoplastic starch and steam exploded cellulose nanofibrils from wheat straw

Anupama Kaushik[a,*], Mandeep Singh[b], Gaurav Verma[a]

[a] University Institute of Chemical Engineering and Technology, Panjab University, Sector 14, Chandigarh 160014, India
[b] Centre for Emerging Areas in Science & Technology, Panjab University, Chandigarh, India

ARTICLE INFO

Article history:
Received 8 November 2009
Received in revised form 9 January 2010
Accepted 23 April 2010
Available online 31 May 2010

Keywords:
Wheat straw
Cellulose nanofibrils
Thermoplastic starch
TGA
DMA
Tensile modulus
Barrier properties

ABSTRACT

The objective was to characterize the properties of cellulose nanofibril/TPS based nanocomposites. The cellulose nanofibrils were extracted from wheat straw using steam explosion, acidic treatment and high shear mechanical treatment. These nanofibrils were dispersed in thermo plastic starch (TPS) using a Fluko high shear mixer in varying proportions and films were casted out of these nanocomposites. The cellulose nanofibrils were characterized using AFM, TEM, SEM, TGA, FTIR and WAXRD and the nanocomposite films were analyzed in terms of SEM, WAXRD, TGA, DSC, mechanical and barrier properties. XRD and TGA results confirmed the crystalline nature of nanofibrils. AFM and TEM images revealed fiber diameter in the range 30–70 nm. TGA depicted an increasing in residue left with increase in cellulose nanofibrils content. Mechanical properties increased with nanofiber concentration. Barrier properties also improved with addition of nanofillers up to 10% but further addition deteriorated properties due to possible fiber agglomeration.

1. Introduction

Growing environmental concerns have created an urgent need to develop biodegradable materials that have comparable properties to polymeric materials at an equivalent cost. Natural biopolymers have an advantage over synthetic biodegradable polymers as they are renewable raw materials.

Starch based biodegradable polymers have great commercial potential for bio-plastic, but some of the properties like brittleness, low heat distortion temperature, high gas permeability, low melt viscosity for further processing, etc. restrict their use in a wide-range of applications. Therefore, modification of the biodegradable polymers through innovative technology is a challenge for materials scientists. Adding nano-reinforcement to pristine polymers to preparing nanocomposite has already proven to be an effective way to improve these properties concurrently (Sinha Ray & Okamoto, 2003). Thus, *green nanocomposites* are being considered as the next generation materials. With the aim of improving thermo-mechanical properties, decreasing water sensitivity of polymers and to preserve the biodegradability, natural fibers are being used as biodegradable fillers. It has been observed that mixing natural fibers with polysaccharides (such as thermoplastic starch) improve their mechanical properties (Curvelo, de Carvalho, & Agnelli, 2001; Dufresne & Vignon, 1998; Dufresne, Cavaillé, & Vignon, 1998).

Cellulose, the building material of long fibrous cells, is a strong natural polymer. Cellulose nanofibers are inherently low cost and are easily available. They are also eco-friendly as they are easy to recycle by combustion, besides consuming less energy during manufacturing. Thus, cellulose nanofiber based composites are an attractive class of nanomaterials on account of low cost, lightweight and high-strength (Helbert, Cavaillé, & Dufresne, 2004; Podsiadlo et al., 2005). Cellulose nanofibers have tremendous attraction due to their unique characteristics such as very large surface to volume ratio, high surface area, good mechanical properties including a high Young's modulus, high tensile strength (Hitoshi & Akira, 2007), low coefficient of thermal expansion (Nishino, Matsuda & Hirao, 2004) and formation of highly porous mesh as compared to other commercial fibers. The supramolecular structure of cellulose determines many of its chemical and physical properties. In the fully extended molecule, adjacent chain units are orientated by their mean planes at an angle of 180° to each other. Thus, the repeating unit in cellulose is the anhydro-cellulobiose unit and number of repeating units per molecule is half the DP. This may be as high as 14,000 in native cellulose, but purification procedures usually reduce it to the order of 2500 (Nevell & Zeronian, 1985).

Various types of cellulosic reinforcements have been used and tested in natural polymers such as potato pulp-based microfibrils (Alain, Danièle, & Michel, 2000; Dufresne & Vignon, 1998) bleached

* Corresponding author. Tel.: +91 172 2534925; fax: +91 172 2779173.
E-mail address: anupamasharma@pu.ac.in (A. Kaushik).

0144-8617/$ – see front matter © 2010 Elsevier Ltd. All rights reserved.
doi:10.1016/j.carbpol.2010.04.063

leafwood fibers (Funke, Bergthaller, & Lindhauer, 1998), bleached eucalyptus pulp fibers (Curvelo et al., 2001), flax fibers and ramie fibers or crystallites (Soykeabkaew, Pitt Supaphol, & Rujiravanit, 2004), tunicin whiskers (Anglès & Dufresne, 2000, 2001), etc. A high compatibility occurs between starch matrix and cellulose nanofibrils with enhanced performance (e.g., mechanical properties and water sensitivity) due to 3D hydrogen bonds network formed between different components.

In the present study, steam treatment with subsequent explosive defibrillation to extract cellulose nanofibrils from wheat straw was performed. The steps include alkaline steam treatment, bleaching and acidic treatment phases followed by mechanical treatment in a high shear homogenizer. Hydrochloric acid has been used for hydrolysis instead of sulfuric acid which is a common choice as it assists with dispersion and separation of nanofibrils due to sulfate ester groups are introduced randomly on the surface resulting in nonflocculating suspensions. For composite applications, the sulfate groups are problematic due to the decreased thermal stability after drying, precluding typical polymer melt processing. Battista and Smith (1962) discovered that formation of stable suspensions can also be achieved by hydrolysis of cellulose using hydrochloric acid followed by mechanical disintegration. The cellulose nanofibrils extracted by above treatment were characterized using TEM, AFM, SEM, FTIR, WAXRD and TGA. These nanofibrils were then reinforced into thermoplastic starch to obtain completely biodegradable nanocomposites by solvent casting in aqueous phase. The nanocomposites so prepared were characterized using SEM, WAXRD, TGA, DSC, Mechanical and their barrier properties studied.

2. Experimental

2.1.1. Materials

Wheat straws were obtained from neighboring fields. They were thoroughly washed to remove any extraneous impurities and dried before use. This is an extremely low cost material which is used for cattle feed. For preparation of thermoplastic starch (TPS), regular maize starch (10% moisture content) of Labochem India Pvt. Ltd. was used along with plasticizer (glycerol) supplied by Swan Scientific, Chandigarh (India). Other chemicals used in the experiment, i.e. sodium hydroxide (NaOH), hydrochloric acid (HCl), hydrogen peroxide (H_2O_2) were supplied by MERCK India Pvt. Ltd.

2.1.2. Extraction of cellulose nanofibrils from wheat straw

2.1.2.1. Alkaline treatment

It was given in two steps. In the first step wheat straw fibers of length around 2–5 cm were soaked in 2% sol. of NaOH overnight and then treated in 10–12% NaOH solution (fiber to liquor ratio around 1:10) in an autoclave at pressure around 15 lb for 4 h. Pressure was then suddenly released resulting in explosive defibrillation of fiber. The first treatment removed excessive impurities from the surface of the fibers and made fibers swollen that made further treatment easy. The second treatment removed excessive amount of lignin from the fibers. The obtained wheat straw pulp was then washed several times in distilled water to get rid of alkali.

2.1.2.2. Bleaching treatment

Alkaline treated pulp was then soaked in 8% solution of H_2O_2 (v/v) overnight. This bleached pulp was then rinsed with abundant distilled water.

2.1.2.3. Acidic treatment

Bleached pulp was treated with 10% HCl (1N) solution and mixed using Branson 2510 E-DTH ultrasonicator at temperature around $60 \pm 1\,^{\circ}C$ for 5 h. Finally the fibers were taken out and washed several times with distilled water in order to neutralize the final pH and then dried.

2.1.2.4. Mechanical treatment

Fibers were suspended in water and continuously stirred with a Fluko FA25 high shear homogenizer for 15 min. High shearing action breaks down the fiber agglomerates and result in nanofibrils.

2.1.3. Preparation of TPS/cellulose nanofibril nanocomposite films

Thermoplastic starch nanocomposites reinforced with cellulose nanofibers (CNFs) extracted from wheat straw were prepared using simple method. Cellulose nanofibers were dispersed in distilled water and sonicated for almost 3 h. Maize starch was added with 30% glycerol and shear mixed for 10 min by using Fluko FA25 homogenizer (10,000 rpm). Dispersion of cellulose nanofibers was added to the starch, glycerol mixer and further shear mixed for 20 min. Starch + glycerol + CNFs mixture was continuously stirred (at 80–100 rpm) using a mechanical stirrer and heated at $75 \pm 3\,^{\circ}C$. After the solution became viscous, it was poured on to leveled Borosil glass petridishes and kept at around 37 °C for 2 days until it was completely dry. Solution cast films of TPS cellulose nanocomposites were made with 5, 10 and 15% nanofibers (as per dry weight of nanocomposites). The film thickness was controlled by pouring calculated amount of mixture on the petridish. The films of thickness approximately 80 μm were obtained and conditioned at 43% RH using saturated solution of $K_2CO_3{\cdot}2H_2O$ at 25 °C for 15 days before testing was done.

2.1.4. Characterization of cellulose nanofibrils and nanocomposites

Chemical composition of fibers was estimated according to the following ASTM procedure: α-cellulose (ASTM D1103-55T), lignin (ASTM D1106-56) and holocellulose (ASTM D1104-56). The standard deviations were calculated by conducting several replicate measurements for each sample. The α-cellulose, hemicelluloses and lignin content were calculated by Eqs. (1)–(3) as follows:

$$\alpha\text{-Cellulose percentage (A)} = \frac{\text{weight of oven dry } \alpha - \text{cellulose residue}}{W \times P} \times 100 \quad (1)$$

$$\text{Hemicellulose percentage} = \frac{\text{weight of oven dry holocellulose residue}}{W \times P} \times 100 - A \quad (2)$$

$$\text{Lignin percentage} = \frac{\text{weight of oven dry lignin residue}}{W \times P} \times 100 \quad (3)$$

where W is the weight of the original oven dry fiber sample and P is the proportion of moisture-free content.

Scanning electron microscope model JSM JEOL-6490 was used for microstructural analysis of cellulose microfibers obtained after steam explosion. Nanocomposite films were frozen in liquid nitrogen and broken into small pieces. Samples were mounted on a metal stub and platinum coated by using sputter coating technique for 20 s to make them conducting. Images of fibers were taken at 20 kV accelerating voltage.

AFM imaging was used to characterize the dimensions and homogeneity of cellulose nanofibrils obtained after chemical and mechanical treatment. The images were scanned in tapping mode in air using silicon cantilevers (Bioscope II AFM, VEECO). Drive frequency of the cantilever was about 200–300 kHz with scan rate of

0.5–3 Hz (usually around 2 Hz). The sample size of 10 μm × 10 μm (Fig. 2a), 1.5 μm × 1.5 μm (Fig. 2b) with the *z* scale of 100 nm was taken. No image processing except flattening was made. Samples were fixed on metal discs with double-sided adhesive tape.

Cellulose nanofibers (CNFs) extracted from wheat straw were examined by using transmission electron microscope (TEM) model Hitachi-2100. Images were taken at 80 kV accelerating voltage. A drop of a dilute aqueous cellulose nanofiber suspension was deposited on the carbon-coated grids and allowed to dry at room temperature. The fiber diameter measurements of the wheat straw fibers after the chemical and mechanical treatment were undertaken using a UTHSCSA Image Tool image analyzer program (IT version 3). The TEM images of the cellulose nanofibers were used to measure the diameters. The images were loaded into the software and diameters of the fibers were measured using a two point measuring analysis. The scale of the software was calibrated using the scale bars on each TEM image (given below each TEM image). Approximately, 300 measurements were taken to obtain each fiber diameter distribution.

FTIR analysis of raw wheat as well as chemically treated wheat straw fibers was done in order to obtain molecular fingerprint of the sample. A Perkin Elmer RX infrared spectrophotometer was used to obtain spectra. Fibers were ground and mixed with KBr (sample/KBr ratio, 1/99) to prepare pastilles. FTIR spectra were recorded in a spectral range of 4000–450 cm^{-1} with a resolution of 2 cm^{-1} with a total of 4 scans for each sample.

X-ray diffraction (WAXRD) profiles of wheat straw fibers before and after the chemical process were collected in order to examine the crystallinity of the samples. The samples were taken in powdered form and analyzed by using a Philips X'Pert Pro X-ray diffractometer system. The radiation was Cu Kα (λ = 1.54060 Å) with 40 kV voltage and 40 mA intensity. Crystallinity of cellulose in pulp samples was calculated from diffraction intensity data. The major diffraction planes of cellulose namely 1 0 1, 1 0 $\bar{1}$, 0 2 1, 0 0 2 and 0 4 0 are present at 14.8°, 16.7°, 20.7°, 22.5°, 34.6° 2θ angle (Krassig, 1985). Crystallinity index was obtained using Eq. (4) (Segal, Creely, Martin, & Conrad, 1959):

$$\text{Crystallinity index} = 100 \times \frac{I_{002} - I_{\text{Amorph}}}{I_{002}} \quad (4)$$

where I_{002} is the maximum intensity of the (0 0 2) lattice diffraction and I_{Amorph} is the diffraction intensity at $2\theta = 18°$. WAXRD of nanocomposite film was also conducted by subjecting the films to X-ray radiation at room temperature.

Thermal stability of untreated, chemically treated, cellulose nanofibrils and nanocomposites was determined using a thermogravimetric analyzer (TGA) of type Perkin Elmer STA-6000. It has a weighing capacity of 1500 mg with resolution around 0.1 μg. Samples were taken in a very small quantity (in milligram) in sample cup made of alumina and having maximum capacity around 180 μl. All the tests were performed in nitrogen environment and at heating rate of 10 °C/min.

Differential scanning calorimeter (DSC) analysis of the composites reinforced with cellulose nanofibers (CNFs) was undertaken on the fractured pieces of samples using a General DSC 2910 TA instrument fitted with refrigeration system and purging gas as nitrogen. Measurements were carried out in temperature range 0–250 °C at scanning rate of 10 °C/min. Conditioned samples of nanocomposites were placed in pressure tight DSC cell and at least three measurements were made to ensure reproducibility. The melting temperature T_m was taken as peak of the melting endotherm.

Tensile testing of the nanocomposites was carried out using universal tensile testing machine Instron 4466 with a load cell of 10 kN and following ASTM D 638. The crosshead speed was set to 2 mm/min. The samples were cut in a dumbbell shape with an ASTM D 638 (type V). Four to five specimens were tested for each sample and average value was taken.

Dynamic mechanical properties of the nanocomposite films were measured using Dynamic Rheometer (TA Instruments, Model Gemini Research Grade GEM 5025) under oscillatory mode. The measurements were performed at a constant frequency of 1 Hz, and strain amplitude of 0.01%. The temperature range was set from room temperature to 200 °C with a heating rate of 3 °C/min. The samples were cut into small strips (40 mm × 10 mm) and conditioned at 43% relative humidity for three weeks. All the tests were performed four times and average value has been reported.

Moisture absorption measurements were performed under 75% relative humidity (NaCl) at 25 °C. All specimens for moisture absorption experiments with dimensions of 30 mm × 10 mm were cut from composite sheets. Prior to absorption experiments, all specimens were vacuum dried until a constant weight was attained. The conditioning of samples in high moisture atmosphere was preferred to the classical technique of immersion of samples in water as starch is very sensitive to water and can partially dissolve after long time exposure to water. At predetermined intervals, specimens were taken out from the chambers and weighed using a Sartorius model analytical balance (with a precision of 0.1 mg). The moisture uptake at any point of time was determined by Eq. (5):

$$\text{Percentage moisture uptake} = \frac{W_h - W_o}{W_o} \times 100 \quad (5)$$

where W_h and W_o denote the weight of humid specimens and the original dry value (the initial weight of materials prior to exposure to moisture absorption), respectively. Data was collected till no successive change in weight was observed. An average of three repeated tests was taken.

3. Results and discussion

3.1. Morphology and chemical characterization of fibers and nanocomposites

Table 1 shows the chemical composition of raw, alkaline steam exploded, bleached and acidic treated fibers. Raw fiber has the highest percentage of hemicellulose and lignin, and the lowest percentage of α-cellulose as compared to treated fibers. The α-cellulose content increases from 45.7% in raw fiber to 86.38% in finally treated fiber. Similarly, hemicellulose content decreases from 37.12 to 8.13% and lignin decreases from 17.43 to 6.34% (Table 1). When the steam explosion process is done, there is a decrease in the hemicellulose and lignin components present in the wheat fiber. This shows that during steam explosion, substantial breakdown of the lignocellulosic structure, partial hydrolysis of the hemicellulosic fraction, and depolymerization of the lignin components has occurred (Cherian et al., 2008).

Fig. 1 shows FTIR spectrum of the raw wheat straw fibers and chemically treated fibers. Peaks in area 3369 cm^{-1} correspond to O–H stretch band, i.e. due to vibrations of the hydrogen bonded hydroxyl (OH) group (Sain & Panthapulakkal, 2006; Sun, Xu, Sun, Fowler & Baird, 2005; Xiao, Sun & Run, 2001). The peaks at 2922 cm^{-1} are due to the aliphatic saturated C–H stretching vibration in lignin polysaccharides (cellulose and hemicelluloses). The hydrophilic tendency of raw wheat straw fibers and chemically treated fibers is reflected in the broad absorption band in the 3700–3100 cm^{-1} region, which is related to the –OH groups present in their main components. The peak at 1734 cm^{-1} in the untreated wheat straw is attributed to either the acetyl and uronic ester groups of the hemicelluloses or the ester linkage of carboxylic group of the ferulic and p-coumeric acids of lignin and/or hemicelluloses (Alemdar & Sain, 2008; Cherian et al., 2008; Sun et al., 2005). This peak is almost absent in the spectra of the chemically

Table 1
Chemical composition of untreated and steam exploded and chemically treated wheat straw.

Material	Percentage of α-cellulose	Percentage of hemi cellulose	Percentage of lignin
Untreated wheat straw	45.70 ± 0.18	37.12 ± 0.9	17.43 ± 2.1
Alkaline steam exploded	65.29 ± 2.51	22.22 ± 1.12	10.27 ± 1.67
Bleached fibers	75.28 ± 2.37	12.34 ± 1.18	8.12 ± 1.35
Acid and alkaline treated fibers	86.38 ± 3.12	8.13 ± 0.8	6.34 ± 1.25

treated fibers which indicates nearly complete cleavage of these ester bonds. The peak at 1652 cm^{-1} may be due to the bending mode of the absorbed water and some contributions from carboxylate groups (Sun et al., 2005). The aromatic C=C stretch from aromatic ring of lignin gives two peaks at 1510 and 1426 cm^{-1} as seen for untreated wheat straw fibers (Alemdar & Sain, 2008; Cherian et al., 2008; Waleed & Maha, 2003). The peak at 1510 cm^{-1} has almost vanished and the intensity of peak at 1426 cm^{-1} has significantly decreased in chemically treated fibers reflecting partial removal of lignin. The peaks at 1373 cm^{-1} represent C–H asymmetric deformation. The intensity of the peak at 1258 cm^{-1} has sharply decreased after chemical treatment indicating the removal of hemicelluloses. The region of 1200–1059 cm^{-1} represents the C–O stretch band and deformation bands in cellulose, lignin and residual hemicelluloses (Sun et al., 2005). The increase of band at 897 cm^{-1} in chemically treated wheat straw fibers indicates the typical structure of cellulose (due to β-glycosidic linkages of glucose ring of cellulose) (Gañán, Cruz, Garbizu, Arbelaiz & Mondragon, 2004).

The alkaline steam explosion results in structural as well as chemical changes on the fiber surfaces. SEM pictures of the wheat straw before and after steam explosion were taken to investigate the change in structure of these fibers (Fig. 2a and b). Fig. 2a shows the native fiber bundles of plant cell with certain surface impurities. Fig. 2b clearly shows individual fibers after the removal of hemicellulose, lignin and pectin after chemical treatment, which are the cementing material around the fiber bundles. Average diameter of the fibers is about 10–15 μm, which is lower than the average size of fiber bundles before chemical treatment.

Fig. 2c shows TEM images of the cellulose nanofibers after the chemical and mechanical treatment. Mechanical treatment resulted in defibrillation of the cellulose nanofibers from the cell wall and TEM images reveal the separation of these nanofibers from the microsizes fiber bundles. Diameter of the fibers was found to be in the range of 10–60 nm. A tendency of agglomeration was also observed from TEM. The average diameter was calculated from the electron micrographs using digital image analysis software, UTHSCSA. Most of the particles were found in the diameter range 30–40 nm. Only 3% of fibers have diameter >70 nm. Almost 64% of fibers have diameter between 30 and 50 nm and 19% less than 30 nm.

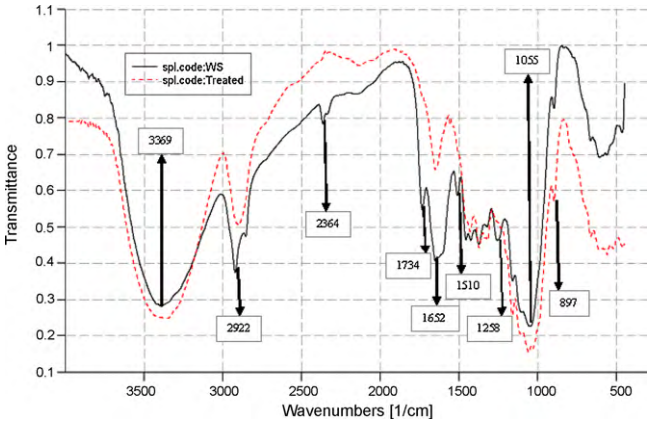

Fig. 1. FTIR spectra of wheat straw fibers (untreated and chemically treated).

Fig. 2d and e is AFM phase images of the nanofibers extracted. The results reveal that fiber diameter has reduced to the nanometer range after chemical and mechanical treatment. AFM photographs, revealed fibers to be slightly agglomerated with smooth surface in contrast to rough surface of microfibrils as seen in SEM images. Fig. 2f–i shows SEM pictures of starch cellulose nanocomposites with 10% cellulose nanofibrils. Fig. 2f is taken on the surface and Fig. 2g–i is micrographs of fractured surface. From the image, it is clear that the nanofibers are well dispersed and covered by the matrix. Fiber bundles can be observed embedded in the polymer matrix (as shown by the arrows in Fig. 2f). No fiber pull-out or debonding was observed because of the fine adhesion between the nanofibers and the polymer matrix. Thus these fibers can be used in composites and will result in improvement of mechanical and thermal properties if reinforced in TPS.

3.2. Crystallinity of cellulose nanofibrils and nanocomposites

Fig. 3a reflects XRD profiles of the untreated, chemically treated fibers and cellulose nanofibrils after mechanical shear treatment. Finally treated cellulose nanofibrils show crystalline nature. The peak intensity at $2\theta = 22.6^{\circ}$ corresponding to 002 lattice plane increases with chemical treatment. It further increases sharply with high shear mechanical treatment. Chemically treated fibers show a narrow peak at 26.5°. Some authors have reported it as 002 diffraction (Wan et al., 2006). Higher crystallinity is due to efficient removal of nanocellulosic polysaccharides and dissolution of amorphous zones. The results also confirm that hydrolysis takes place preferentially in the amorphous region due to acidic dissolution while crystalline regions are more stable towards chemical attack. This increase of crystallinity after acid treatment has been extensively reported (Alemdar & Sain, 2008; Cherian et al., 2008; Tang et al., 1996). Crystallinity increases from 54.42% for untreated fibers to 66.60% for chemically treated fibers and to 79.87% for cellulose nanofibrils.

Fig. 3b shows the WAXRD profile for TPS/cellulose nanocomposites. Typical starch granules involve alternating amorphous and crystalline lamellae in which two main components, amylose and amylopectin are embedded. When starch granules are destroyed by heat and shear force during processing, amylose, an essentially linear polymer dissociates out of the granule and crystallizes into several single helical crystal structures. Thermoplastic starch is characterized by a broad hump centered on 19°, revealing that the material is fully amorphous (Angellier, Molina-Boisseau, Dole, & Dufresne, 2006). This shows that the crystalline structure of native starch granules has disappeared during the processing. The magnitude of the peaks at 16.7° and 22.5° increases with the increase in the cellulose nanofibril content, revealing crystalline structure with preservation of the crystallinity of starch nanocrystals during the processing method.

3.3. Thermal properties of nanofibrils and nanocomposites

The TGA results for wheat straw fibers at different stages are shown in Fig. 4a. These results clearly show that thermal stabil-

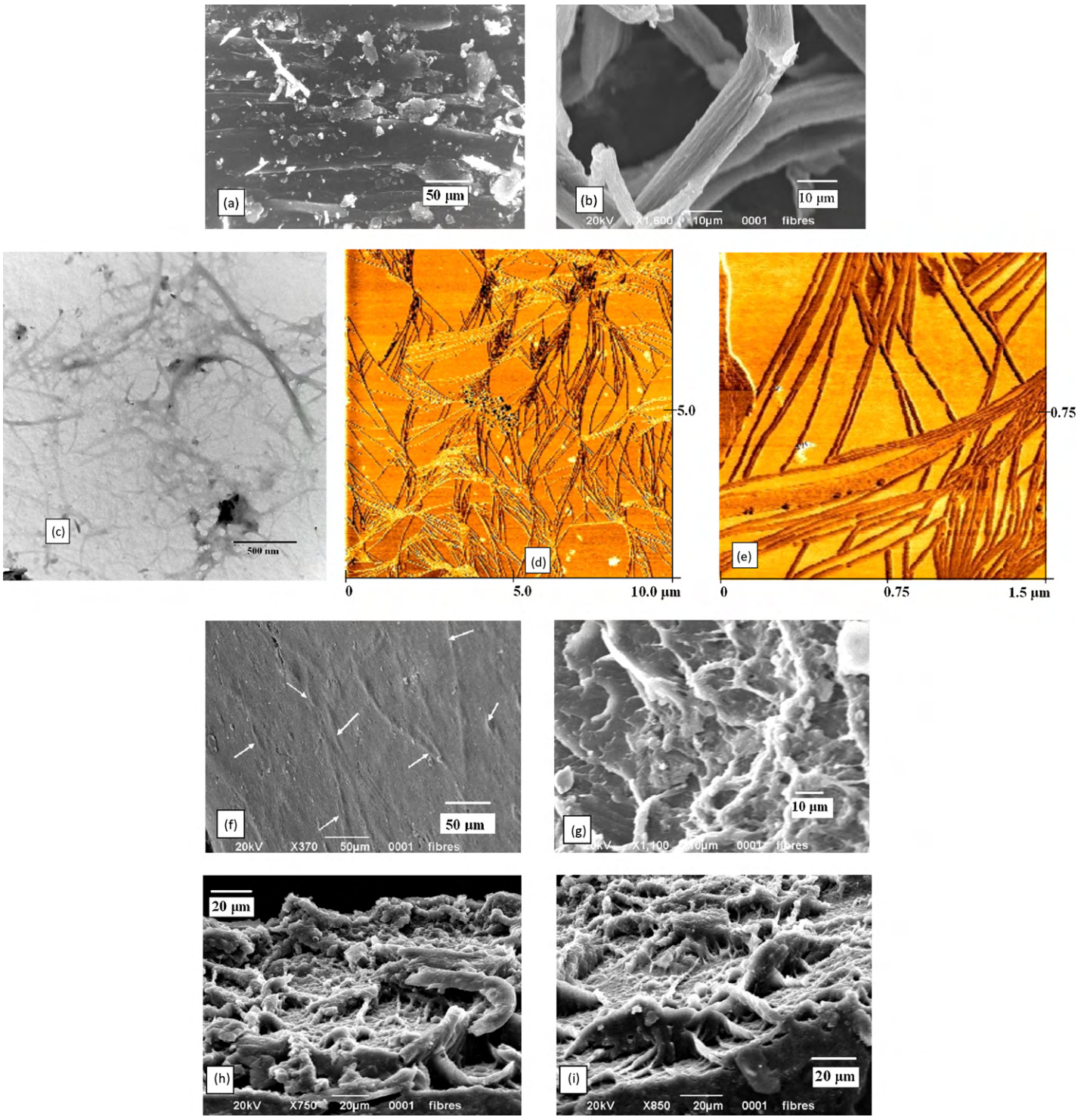

Fig. 2. SEM image of microfibrils (a) before and (b) after steam explosion. (c) TEM images and (d) and (e) AFM images of chemically and mechanically treated cellulose nanofibrils. (f–i) SEM images of starch cellulose nanofibril nanocomposites with 10% cellulose nanofibrils.

Table 2
Decomposition characteristics of wheat straw, chemically treated fibers and nanofibrils.

Fiber type	T_o (°C)	T_p (°C)	Weight loss at T_o (MT_o) (%)	Weight loss at T_p (MT_p) (%)	%age residue at T_{600} (MT_{600}) (%)
WS	239.5	321.86	6.54	27.81	78.42
CTWS	276.2	345.71	7.35	49.88	82.45
CNF	283.2	337.58	6.876	23.49	89.01

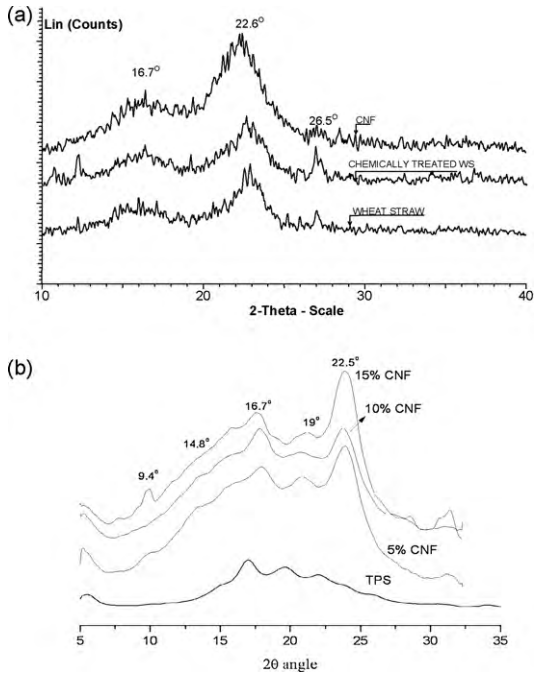

Fig. 3. (a) XRD spectra of different fibers: (i) untreated wheat straw; (ii) chemically treated wheat straw; (iii) cellulose nanofibrils. (b) XRD spectra of TPS cellulose nanofibril nanocomposites with 5, 10 and 15% nanofibrils.

ity of the wheat straw fibers increases after chemical treatment as well as high shear mechanical treatment. The degradation temperature increased after chemical treatment. This was probably because more non-cellulosic material was removed and high degree of structural order retained. This revealed a relationship between the structure and thermal degradation of cellulose. A greater crystalline structure required a higher degradation temperature (Ouajai & Shanks, 2005). However, both non-cellulosic components and the crystalline order of cellulose played an important role in thermal degradation of the fibers (Yang & Kokot, 1996). The decomposition characteristics of wheat straw, chemically treated and high shear mechanically treated fibers are summarized in Table 2. T_o represents the onset temperature and T_p, the peak temperature of thermal decomposition. MT_o and MT_p are percentage weight loss at T_o and T_p. The residual solid mass fraction percentage left at the final temperature, 600 °C is marked as MT_{600}. The residual weight was the maximum for wheat straw (22%) followed by chemically treated fibers (18%). Minimum residual weight was 11% after mechanical high shear treatment. This is because of absence of non-organic components in the cellulose nanofibrils as confirmed by FTIR and XRD analysis.

Fig. 4b shows TGA results of TPS cellulose nanocomposites with 5, 10 and 15% cellulose nanofibrils. Onset temperature of starch degradation is found to be around 273 °C and that of cellulose nanofibrils 283.2 °C (Fig. 4a). Change in onset temperature with increase in cellulose content is insignificant except for nanocomposite containing 15% CNF, which is less than that of TPS and is around 255 °C. This may be the outcome of decrease in flexibility of amylopectin chains in the presence of crystalline cellulose. Another reason may be accumulation of glycerol on the surface of cellulose nanofibrils. The accumulation of plasticizer in the cellulose/amylopectin interfacial zone improves the ability of amylopectin chains to crystallize leading to the formation of possible crystalline zone around the fibrils (Anglès & Dufresne, 2000). This is also referred as anti-plasticization of amylopectin-rich domains of starch (Kumar & Singh, 2008).

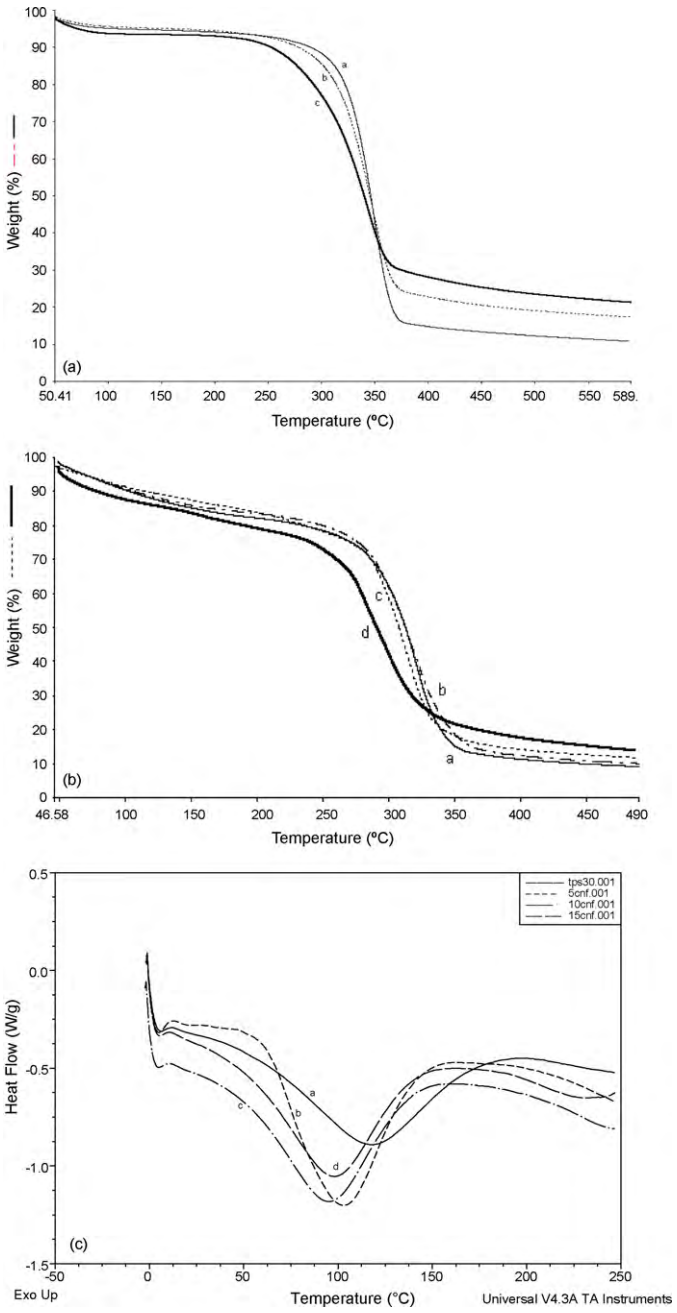

Fig. 4. (a) TG curves: (a) finally mechanical treated fibers, (b) after acidic treatment and (c) wheat straw. (b) TG curves of TPS cellulose nanofibril nanocomposites: (a) TPS, (b) 5% CNF, (c) 10% CNF and (d) 15% CNF. (c) DSC plots of: (a) neat TPS, (b) 5 wt%, (c) 10 wt% and (d) 15 wt% CNFs filled TPS nanocomposites.

The percent residue increases with increase in CNF content. This is due to cellulose-based composites having a lower water content at equilibrium, compared to unfilled TPS. As cellulose is crystalline, its crystallinity decreases the polar character of starch. Thus, the addition of cellulose into a starchy matrix decreases the global water content with resultant increase in the CNF content (Avérous, Fringant, & Moro, 2001).

Fig. 4c shows the DSC curves for TPS and nanocomposites. Melting temperature (T_m) and heat of fusion (ΔH_m) were determined for all the samples on the first heating run. It has been observed that enthalpy of fusion is larger for composites filled with fibers than neat TPS film, decreasing with the increase in the fiber content. For neat TPS film ΔH_m was 171 J/g. Heat of fusion was 197 J/g

for 5% fibers, 190 J/g for 10% fibers and 169 J/g for 15% fibers. On the contrary, melting point temperature of fiber filled composites dropped from 118.67 °C for neat TPS film to 98.57 °C for film containing 15% fibers. Melting point of composites containing 5 and 10% fibers was 103.32 and 95.89 °C, respectively. Nanocomposite with 5% fiber showed maximum heat of fusion due to its well dispersed filler morphology. Higher filler dispersion and interfacial adhesion hinders to some extent lateral rearrangements of polymer chains and hence crystallization of these materials. The results are also supported by TGA.

3.4. Mechanical properties of nanocomposites

The tensile properties of the nanocomposite films were analyzed and stress–strain curves were obtained at 30 °C and 50% relative humidity. Fig. 5a shows the reinforcing ability of the cellulose nanofibrils by means of tensile modulus and yield strength. The tensile strength and modulus of the nanocomposite films increased linearly with the increase in CNF content. The nanocomposite with 15% fiber loading showed an improvement of 195% over pure TPS. Tensile test results indicate good bonding and efficient stress transfer from matrix to fiber. The enhancements in toughness of the composites with the addition of cellulose nanofibrils is quite evident in Fig. 5a, the increases in both modulus and strain at fracture resulted in improvements in ultimate strength of the composites. In cellulose-based nanocomposites, the unusual reinforcement effect obtained by nano-sized elements is attributable to the formation of a rigid network of nanofibers connected by hydrogen bonds and also by mutual entanglements (Siqueira, Bras & Dufresne, 2009).

DMA is often used to study relaxations in polymers. An analysis of storage modulus, loss modulus, and tan δ is very useful in ascertaining the performance of a sample with varying temperature. Storage modulus (E') of TPS and nanocomposites as a function of temperature is given in Fig. 5b. The storage modulus of the nanocomposites increased with increasing CNF content as compared to the TPS. There was a continuing decrease in modulus as a function of temperature. The storage modulus decreased significantly with temperature for TPS and nanocomposite with 5% fibers. For nanocomposite with 15% CNF, the decrease of modulus with temperature was significantly less showing an improvement in mechanical property with addition of CNF. Values of storage modulus at 30 °C and tan δ peak values for different nanocomposite films are reported in Table 3. The relaxation peaks (tan δ) shifted to higher temperatures, broadened and diminished their intensity with increasing in CNF content. Shift of the relaxation to higher temperatures is associated with the decreased mobility of the polymer chain as it happens with addition of any filler. The temperature shift is quite remarkable, about 30–40 °C, and indicates that nanofibers were able to affect segmental motions of the TPS. It is pertinent to note that filler addition can exert different effects on tan δ: it can increase the interfacial area, producing an increase in tan δ while producing a decrease in moisture content, thereby reducing the internal friction. In the present study, the first effect seems to predominate. Additionally, relaxation temperature of thermoplastic starch depends on the plasticizer content, humidity conditions as well as the composition of the starch. In the literature, there are variations in T_g values as even for the same glycerol content (Mathew & Dufresne, 2002a, 2002b). This can explained by differences in the preparation conditions of the TPS.

3.5. Moisture retention properties of nanocomposites

Starch is an abundant biopolymer but has poor moisture resistance. Addition of nanofibers is an effective way of decreasing its sensitivity to moisture and thus improving mechanical properties

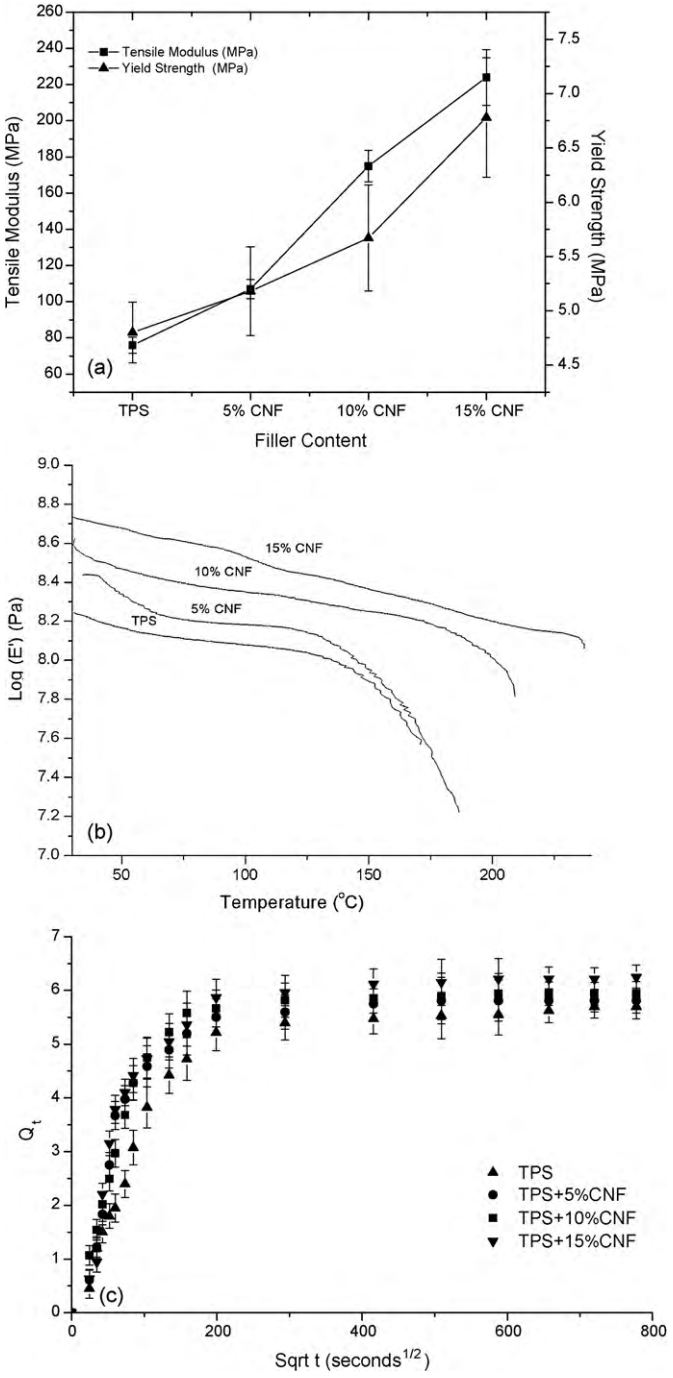

Fig. 5. (a) Tensile modulus (MPa), yield strength (MPa) for TPS and TPS cellulose nanofibril nanocomposites. (b) Temperature dependence of storage modulus for TPS and TPS cellulose nanofibril nanocomposites. (c) Moisture absorption curves of TPS and TPS cellulose nanofibril nanocomposites in 75% RH.

and stability. Although cellulose and starch are both hydrophilic but functional groups present on surface of both cellulose and starch result in good interfacial adhesion between the two molecules thereby increasing water resistance and mechanical properties. Moreover, cellulose nanofibers are less hygroscopic than starch due to higher degree of molecular order making them effective in improving the barrier properties. Theoretically, moisture absorption processes in polymer composites, mostly from conventional non-biodegradable composites, can be described by Fick's second law of diffusion. General series solution of the Fick second law for plane sheet geometry with the assumptions of molecular migra-

Table 3
Mechanical properties and Barrier properties (75% RH) for various thermoplastic starch/cellulose nanofibril nanocomposites.

Mechanical properties					Barrier properties				
Cellulose nanofibril content	Tensile modulus (MPa)	Yield strength (MPa)	Storage modulus at room temperature (30 °C) (MPa)	Tan δ peak (°C)	k ($s^{-1/2}$)	M_∞ (%)	D ($\times 10^{-4}$ mm^2 s^{-1})	$S \times 10^{-2}$	P (mm^2 s^{-1})
0%	76 ± 4.5	4.8 ± 0.28	142	102	0.74	5.93 ± 0.14	7.71 ± 0.10	5.93 ± 0.04	0.45 ± 0.06
5%	107 ± 5.3	5.18 ± 0.41	149	122	0.66	5.81 ± 0.11	6.41 ± 0.08	5.81 ± 0.04	0.37 ± 0.08
10%	175 ± 8.7	5.67 ± 0.49	301	138	0.56	5.69 ± 0.09	4.80 ± 0.09	5.69 ± 0.05	0.27 ± 0.10
15%	224 ± 15.4	6.78 ± 0.55	486	142	0.78	6.24 ± 0.12	7.80 ± 0.11	6.24 ± .06	0.48 ± 0.11

tion by diffusion, negligible shrinkage besides constant diffusion and temperature is given by equation 6 (Crank, 1975):

$$\frac{M_t}{M_\infty} = 1 - \frac{8}{\pi^2}\sum_{\pi^2}^{8}\frac{1}{(2n+1)^2}\ \exp\left[-\left(\frac{D(2n+1)^2 t}{h^2}\right)\pi^2\right] \quad (6)$$

where M_t and M_∞ are the moisture contents at time t and at equilibrium, respectively. D is the diffusion coefficient and h is the sample thickness. At short times, i.e., the initial absorption (initial linear portion of the curve) ($M_t/M_\infty \leq 0.5$) Eq. (6) reduces to:

$$\frac{M_t}{M_\infty} = \left(\frac{4}{h}\right)\left(\frac{d}{\pi}\right)^{1/2} t^{1/2} \quad (7)$$

Eq. (7) can be rewritten as:

$$M_t = kt^{1/2} \quad (8)$$

where k is the slope of M_t vs. $t^{1/2}$ curve:

$$k = \left(\frac{4M_\infty}{h}\right)\left(\frac{D}{\pi}\right)^{1/2} \quad (9)$$

Hence D can be calculated from the slope of M_t vs. $t^{1/2}$ curve for known thickness of the sample. The sorption coefficient S is given by Eq. (10):

$$S = \frac{m_\infty}{m_p} \quad (10)$$

where m_∞ represents mass of the solvent taken up at the equilibrium and m_p represents initial mass of the sample. The permeability coefficient (P), which gives a combined effect of both D and S, was also calculated using the equation $P = D \times S$.

In this study moisture absorption behavior of nanocomposites was studied at 25 °C for 75% RH. Fig. 5c shows the moisture uptake of TPS and cellulose nanofibrils/TPS nanocomposites with varying fiber loading as a function of time. The values of typical kinetic parameters, M_∞, k, D, S and P obtained in this study are summarized in Table 3. It is observed that the thermoplastic sheet of corn starch absorbs about 5.93 wt.% water. The moisture uptake at equilibrium, M_∞, decreases with increasing cellulose nanofibril loading, and about 5.69 wt.% of water uptake is observed for 10% cellulose nanofibril loading (Fig. 5c). The diffusivity decreases from 7.71×10^{-4} mm^2 s^{-1} for pure TPS film to 4.80×10^{-4} mm^2 s^{-1} for film containing 10% CNF. High value of diffusivity of pure starch is due to its hygroscopic nature making it prone to moisture absorption. The diffusivity decreases because at higher levels of fiber loading, lower water diffusion was found ascribed to the hydrogen bond formed between the matrix phase and the fiber phase within the composite (Sreekala, Goda & Devi, 2008). The presence of strong hydrogen bonding interactions between starch and cellulose crystallites decrease diffusivity since the hydrogen bonding interactions in the composites tend to stabilize starch matrix when it is submitted to high humidity atmosphere. The reduction in permeability is strongly related to a reduction in the diffusion coefficient imposed by the presence of the fibers but also to a decrease in sorption of the penetrant. However, if we increase the CNF loading above 10%, the diffusivity increases sharply and so is M_∞. As increasing fiber content results in fiber agglomeration, there is reduction in matrix homogeneity and cohesion. This leads to preferential penetrant path and to detrimental effect on barrier properties (Sanchez-Garcia, Gimenez & Lagaron, 2008). Similar behavior has been observed by other authors at high fiber loading (Mathew & Dufresne, 2002a). This behavior can be explained on the basis of two opposite factors (Mathew & Dufresne, 2002a). One the one hand, the increase in cellulose fibril content leads to the formation of denser microcrystal network thereby increasing the mechanical properties. This dense network should decrease the diffusivity through the sample. On the other hand, by increasing the fiber content, the proportion of microcrystals positioning at the surface increases continuously. If the adhesion level between the filler and matrix is not good, it can create diffusion pathways which tend to increase diffusivity of water. If this explanation is valid, this effect predominate around 10% fiber content. In the present study, this behavior is evident at 15% fiber content. A second possible explanation of decrease in diffusivity is due to change in relaxation temperature because of reduced segmental mobility of polymer molecules at high fiber loading (10–15%).

4. Conclusions

Green nanocomposites were obtained from glycerol plasticized corn starch as the matrix and steam exploded cellulose nanofibrils from wheat straw. TEM, SEM and AFM confirmed the nano-size of the fibers. XRD results of nanocomposites reveal improvement in crystallinity with addition of nanofibrils. The results of TGA and DSC experiments indicated an interaction between the fiber and the plasticizer, causing the reduction in onset of degradation temperatures and a reduction in water sorption compared to the pure matrix. Mechanical properties including DMA and tensile modulus showed marked improvement with addition of CNF. These nanofibers offer potential for reinforcing polymer composites.

Acknowledgements

We gratefully acknowledge financial support rendered by All India Council of Technical Education (AICTE), India and University Grants Commission (UGC), India for the research work.

References

Alain, D., Danièle, D., & Michel, R. V. (2000). Cellulose microfibrils from potato tuber cells: processing and characterization of starch–cellulose microfibril composites. *Journal of Applied Polymer Science*, *76*(14), 2080–2092.

Alemdar, A., & Sain, M. (2008). Isolation and characterization of nanofibers from agricultural residues—wheat straw and soy hulls. *Bioresource Technology*, *99*(6), 1664–1671.

Angellier, H., Molina-Boisseau, S., Dole, P., & Dufresne, A. (2006). Thermoplastic starch waxy maize starch nanocrystals nanocomposites. *Biomacromolecules*, *7*(2), 531–539.

Anglès, M. N., & Dufresne, A. (2000). Plasticized starch/tunicin whiskers nanocomposites. 1. Structural analysis. *Macromolecules*, *33*(22), 8344–8353.

Anglès, M. N., & Dufresne, A. (2001). Plasticized starch/tunicin whiskers nanocomposite materials. 2. Mechanical behavior. *Macromolecules*, *34*(9), 2921–2931.

Avérous, L., Fringant, C., & Moro, L. (2001). Plasticized starch–cellulose interactions in polysaccharide composites. *Polymer Composites*, *42*(15), 6571–6578.
Battista, O. A., & Smith, P. A. (1962). Microcrystalline cellulose. *Industrial & Engineering Chemistry*, *54*(9), 20–29.
Cherian, B. M., Pothan, L. A., Nguyen-Chung, T., Mennig, G., Kottaisamy, M., & Thomas, S. (2008). A novel method for the synthesis of cellulose nanofibril whiskers from banana fibers and characterization. *Journal of Agricultural and Food Chemistry*, *56*(14), 5617–5627.
Crank, J. (1975). *The mathematic of diffusion*. London, UK: Oxford University Press.
Curvelo, A. A. S., de Carvalho, A. J. F., & Agnelli, J. A. M. (2001). Thermoplastic starch–cellulosic fibre composites: preliminary results. *Carbohydrate Polymers*, *45*(2), 183–188.
Dufresne, A., Cavaillé, J.-Y., & Vignon, M. R. (1998). Mechanical behavior of sheets prepared from sugar beet cellulose microfibrils. *Journal of Applied Polymer Science*, *64*(6), 1185–1194.
Dufresne, A., & Vignon, M. R. (1998). Improvement of starch film performances using cellulose microfibrils. *Macromolecules*, *31*(8), 2693–2696.
Funke, U., Bergthaller, W., & Lindhauer, M. G. (1998). Processing and characterization of biodegradable products based on starch. *Polymer Degradation and Stability*, *59*(1–3), 293–296.
Gañán, P., Cruz, J., Garbizu, S., Arbelaiz, A., & Mondragon, I. (2004). Stem and bunch banana fibers from cultivation wastes: effect of treatments on physico-chemical behavior. *Journal of Applied Polymer Science*, *94*(4), 1489–1495.
Helbert, W., Cavaillé, J. Y., & Dufresne, A. (2004). Thermoplastic nanocomposites filled with wheat straw cellulose whiskers. Part I: Processing and mechanical behavior. *Polymer Composites*, *17*(4), 604–611.
Hitoshi, T., & Akira, A. (2007). Characterization of "green" composites reinforced by cellulose nanofibers. *Key Engineering Materials*, *334–335*, 389–392.
. (1985). Krassig, H. (Ed.), *Structure of cellulose and its relation to properties of cellulose fibers* Chichester, UK: Ellis Horwood.
Kumar, A. P., & Singh, R. P. (2008). Biocomposites of cellulose reinforced starch: improvement of properties by photo-induced crosslinking. *Bioresource Technology*, *99*(18), 8803–8809.
Mathew, A. P., & Dufresne, A. (2002a). Morphological investigation of nanocomposites from sorbitol plasticized starch and tunicin whiskers. *Biomacromolecules*, *3*(3), 609–617.
Mathew, A. P., & Dufresne, A. (2002b). Plasticized waxy maize starch: effect of polyols and relative humidity on material properties. *Biomacromolecules*, *3*(5), 1101–1108.
Nattakan Soykeabkaew, Pitt Supaphol, & Rujiravanit, R. (2004). Preparation and characterization of jute- and flax-reinforced starch-based composite foams. *Carbohydrate Polymers*, *58*(1), 53–63.
Nevell, T. P., & Zeronian, S. H. (1985). *Cellulose chemistry and its applications*. New York: Wiley.
Nishino, T., Matsuda, I., & Hirao, K. (2004). All-cellulose composite. *Macromolecules*, *37*(20), 7683–7687.
Ouajai, S., & Shanks, R. A. (2005). Composition, structure and thermal degradation of hemp cellulose after chemical treatments. *Polymer Degradation and Stability*, *89*(2), 327–335.
Podsiadlo, P., Cho, S. Y., Shim, B., Lee, J., Cuddihy, M., & Kotov, N. A. (2005). Molecularly engineered nanocomposites: layer-by-layer assembly of cellulose nanocrystals. *Biomacromolecules*, *6*(6), 2914–2918.
Sain, M., & Panthapulakkal, S. (2006). Bioprocess preparation of wheat straw fibers and their characterization. *Industrial Crops and Products*, *23*(1), 1–8.
Sanchez-Garcia, M. D., Gimenez, E., & Lagaron, J. M. (2008). Morphology and barrier properties of solvent cast composites of thermoplastic biopolymers and purified cellulose fibers. *Carbohydrate Polymers*, *71*(2), 235–244.
Segal, L., Creely, J. J., Martin, A. E., Jr., & Conrad, C. M. (1959). An empirical method for estimating the degree of crystallinity of native cellulose using the X-ray diffractometer. *Textile Research Journal*, *29*(10), 786–794.
Sinha Ray, S., & Okamoto, M. (2003). Polymer/layered silicate nanocomposites: a review from preparation to processing. *Progress in Polymer Science*, *28*(11), 1539–1641.
Siqueira, G., Bras, J., & Dufresne, A. (2009). Cellulose whiskers versus microfibrils: influence of the nature of the nanoparticle and its surface functionalization on the thermal and mechanical properties of nanocomposites. *Biomacromolecules*, *10*(2), 425–432.
Sreekala, M. S., Goda, K., & Devi, P. V. (2008). Sorption characteristics of water, oil and diesel in cellulose nanofiber reinforced corn starch resin/ramie fabric composites. *Composite Interfaces*, *15*(2–3), 281–299.
Sun, X. F., Xu, F., Sun, R. C., Fowler, P., & Baird, M. S. (2005). Characteristics of degraded cellulose obtained from steam-exploded wheat straw. *Carbohydrate Research*, *340*(1), 97–106.
Tang, L. C., Hon, D. N. S., Pan, S. H., Zhu, Y. Q., Wang, Z., & Wang, Z. Z. (1996). Evaluation of microcrystalline cellulose. 1. Changes in ultrastructural characteristics during preliminary acid hydrolysis. *Journal of Applied Polymer Science*, *59*(3), 483–488.
Waleed, K. E.-Z., & Maha, M. I. (2003). Synthesis and characterization of cellulose resins. *Polymer for Advanced Technologies*, *14*(9), 623–631.
Wan, Y. Z., Hong, L., Jia, S. R., Huang, Y., Zhu, Y., Wang, Y. L., et al. (2006). Synthesis and characterization of hydroxyapatite–bacterial cellulose nanocomposites. *Composites Science and Technology*, *66*(11–12), 1825–1832.
Xiao, B., Sun, X. F., & Run, C. S. (2001). Chemical, structural, and thermal characterizations of alkali-soluble lignins and hemicelluloses, and cellulose from maize stems, rye straw, and rice straw. *Polymer Degradation and Stability*, *74*(2), 307–319.
Yang, P., & Kokot, S. (1996). Thermal analysis of different cellulosic fabrics. *Journal of Applied Polymer Science*, *60*(8), 1137–1146.